# CVD preparation and characterization of tin dioxide films for electrochemical applications

**F. Javier Yusta, Michael L. Hitchman* and Sarkis H. Shamlian**

*Department of Pure and Applied Chemistry, University of Strathclyde, 295 Cathedral Street, Glasgow, UK G1 1XL*

$SnO_2$ films have been succesfully prepared by chemical vapour deposition (CVD) by reaction of $SnCl_2$ with $O_2$ and a value of the activation energy of 58 kJ $mol^{-1}$ has been measured. The temperature range 450–500 °C has been found to be the optimum for the reaction with resistivities of the films of $9 \times 10^{-4}$ Ω cm on silicon and $6 \times 10^{-4}$ Ω cm on Pyrex. These two values are the lowest reported so far for $SnO_2$ films which have not been deliberately doped. For their use as transparent conducting films, a figure of merit of $9.87 \times 10^{-3}$ □ $\Omega^{-1}$ was found for a 0.8 μm thick film; this is also the highest reported so far. Characterization of the films by XRD showed a preferred [200] orientation and the grain size obtained from the XRD and SEM micrographs was in excess of 0.4 μm. The $SnO_2$ films, when tested in an eletrochemical cell, were unstable. A surface electrochemical process has been suggested for the disintegration.

## 1 Introduction

Tin dioxide ($SnO_2$) is a versatile material whose optical, electrical and mechanical properties have led to it being widely used for various applications. It is a wide band gap (3.7 eV) semiconductor[1] that is an insulator in its stoichiometric form, but due to lattice imperfections and oxygen vacancies arising during its production it becomes n-type and conductive. This conductivity can be increased by the presence of dopants, introduced either non-intentionally, as in the case of Cl (*e.g.* from the most common precursors $SnCl_4$ and $SnCl_2$), or by the deliberate addition of elements such as Sb,[2] In,[3] F,[3] P,[4] B,[5] Mo;[6] the dopants mainly used, though, have been Sb and In to give n- and p-type materials, respectively.[7] Both types have the properties of high conductivity, high transparency in the visible region, and high reflectivity in the IR region.[8] They can be deposited by physical or chemical means, they are stable up to high temperatures, are resistant to strong acids and bases at room temperature, and have a very good adhesion to many substrates (*e.g.* glass, metals and oxides) so that they cannot be peeled off mechanically.[9]

All these properties have made $SnO_2$ an interesting coating for a variety of applications. In recent years the use of $SnO_2$ films as electrodes for electrochemical applications has been studied especially under demanding conditions such as water electrolysis and oxidation and destruction of intractable organic effluents. This has been because of the high chemical and electrochemical stability of the oxide, resulting from the rather large band gap and the high electrical conductivity when doped. $SnO_2$ films also have the advantage of a high catalytic activity for the destruction of aromatics and a high oxygen evolution overpotential which is even higher than that found for Pt and $PbO_2$, both of which, along with graphite, are the most commonly used high oxygen evolution potential anodes for the oxidation of organic molecules.[10] Also platinum, often in the form of platinized titanium which has a less positive oxygen overpotential, has the disadvantage of being expensive, whilst graphite and $PbO_2$ are not stable under normal electrolysis conditions.[10] Unfortunately, however, it has also been reported that $SnO_2$ films disintegrate at the high current densities which are used on an industrial scale.[10,11] We have begun to investigate this problem.

Tin dioxide films can be prepared by a variety of methods such as spray pyrolysis,[10,12] which allows the coating of large surfaces, reactive sputtering,[13,14] reactive evaporation[15,16] and electron-beam evaporation;[17] each of these techniques has advantages and disadvantages. The spray pyrolysis technique is the method which has been mainly used for preparation of electrodes for electrochemical applications but electrodes prepared by this method have limited lifetimes when used in electrochemical cells.[10] Therefore it seemed worthwhile to investigate electrode preparation by CVD which could produce films with improved integrity and adherence.

In this work the CVD of $SnO_2$ films and their characterization and testing for possible use as electrodes for the destruction of organic effluents is reported.

## 2 Experimental

$SnO_2$ layers have previously been produced by CVD from a variety of precursors including organometallics (*e.g.* dibutyltin diacetate[18] and tetramethyltin[9]), tin chlorides and tin iodide.[19] In this work, for reasons of cost and simplicity, only the chlorides of tin were considered. They can be used in one of two different ways

Hydrolysis with water to give HCl:

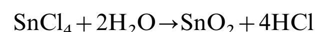

$$SnCl_4 + 2H_2O \rightarrow SnO_2 + 4HCl$$

Oxidation with oxygen to give $Cl_2$:

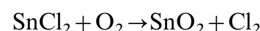

$$SnCl_2 + O_2 \rightarrow SnO_2 + Cl_2$$

The first reaction is commonly used in spray pyrolysis, whereas the second reaction is the one which has produced the best results so far in CVD.[20] Therefore this latter reaction was selected to deposit our $SnO_2$ films. For electrochemical applications Sb doped $SnO_2$ has been mainly used.[10] For CVD doping, antimony organometallics and antimony chlorides are the choices available, and again we have only considered the chlorides. These could be either $SbCl_3$ or $SbCl_5$. The former is a solid at room temperature, whereas the latter is a liquid and so can be readily transported under ambient conditions by an inert gas.

A schematic diagram of the experimental set-up is shown in Fig. 1. The reaction chamber consisted of a 720 mm long quartz tube and with an inner diameter of 55 mm. Around it were placed two furnaces to control the evaporation (furnace 1) and deposition temperatures (furnace 2). These temperatures were controlled by thermocouples in contact with the quartz tube at the positions where the evaporator and substrates were placed. $SnCl_2$ (98% purity, Aldrich) was introduced into the reaction chamber by means of an evaporator, through which the carrier gas ($N_2$) was flowed. Having the evaporator inside

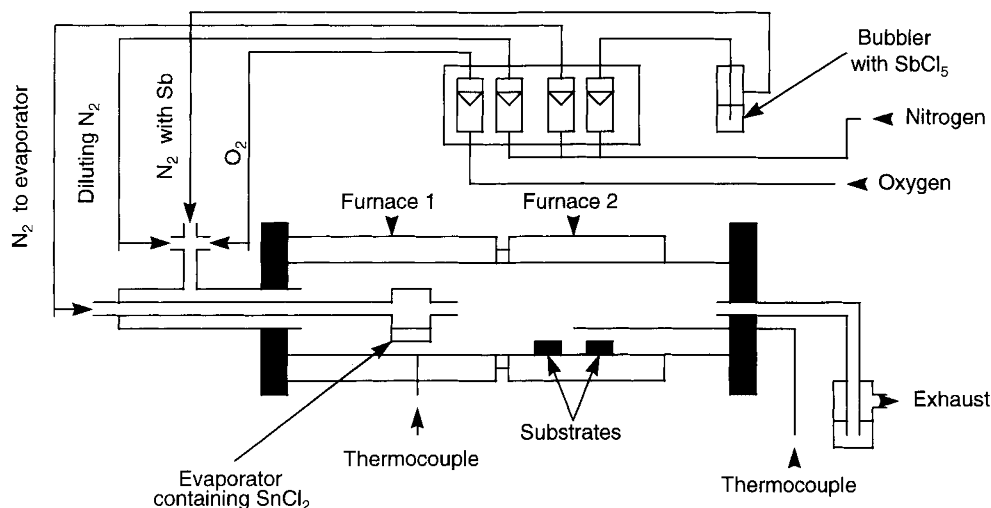


**Fig. 1** Schematic of the deposition system

the reactor tube overcame any problems associated with condensation of the precursor.

$SnO_2$ layers began to appear when the temperature of the quartz in contact with the evaporator was 340 °C, about 90 °C above the melting point of $SnCl_2$. Because the minimum evaporation temperature seemed to vary with time and a blackening of the surface of the precursor was observed, possibly as a result of reaction of $SnCl_2$ with the glass of the evaporator, the $SnCl_2$ was replaced after each experiment. Nitrogen was passed into the reactor to purge it prior to reaction until the required evaporation rate was achieved, and also after reaction to remove $O_2$ in order to stop the reaction. Nitrogen was also used as the carrier gas for the dopant (99% $SbCl_5$, Aldrich) which was contained in a bubbler at 28 °C; this temperature was controlled by a water-bath.

Once the evaporation temperature was achieved, $O_2$ was introduced into the reactor and this introduction defined the start of the reaction. When the desired reaction time was reached nitrogen was flowed into the chamber again, the flow of oxygen was stopped and the evaporation furnace was switched off to stop the evaporation. When the furnace temperature had fallen below 200 °C (about 50 °C below the melting point of $SnCl_2$) the evaporator and samples were removed.

The flows in the various gas lines were regulated by flowmeters. Typical flows for each line were: 50–150 $cm^3$ $min^{-1}$ for the $N_2$ to the evaporator, 0.5–1.0 $dm^3$ $min^{-1}$ for the $N_2$ for dilution, 50–200 $cm^3$ $min^{-1}$ for $N_2$ for doping, and 1–5 $dm^3$ $min^{-1}$ for the $O_2$ for reaction.

The variables, apart from the deposition temperature, were evaporation temperature, location of the evaporator inside the reactor, distance of test samples from the entrance of the reactor, flow of $N_2$ through the evaporator, and flow of $O_2$ through the reaction chamber. The way the effect of all these factors was assessed was to place slices of silicon substrate along the deposition zone of the reactor and to analyse the evolution of conductivity as any of the variables of the system was modified. Optimum values were selected on the basis of layer thickness uniformity between samples and maximum conductivity.

After this process of optimization, the reaction conditions were fixed as follows: evaporation temperature = 500 °C; distance of the evaporator from entrance of reactor = 33.5 cm; distance of test samples from entrance of reactor = 40 or 46 cm; $O_2$ flow = 1 $dm^3$ $mol^{-1}$ and $N_2$ flow through the evaporator = 150 $cm^3$ $mol^{-1}$.

Substrates for the films were silicon wafers for investigating deposition kinetics and electrical properties, borosilicate glasses for monitoring the optical properties, and titanium for electrochemical studies. The size of the substrates was, in general, 1 cm × 2 cm.

Thicknesses were generally measured by an Auto Grain Ellipsometer L116B (Gaertner Scientific Corporation). However, owing to absorbance by thick films, thicknesses of such samples were calculated from the mass difference of the samples as measured with a Mettler microbalance before and after the reaction; a density of $SnO_2$ of 6.9 g $cm^{-3}$ was assumed. Thicknesses were also checked at some stages with a Dektak IIA Sloan profilometer by measuring the step created by etching the layer with a HCl/Zn powder slurry.

The sheet resistance of the films ($\Omega\ \square^{-1}$) was measured by a conventional four-point probe technique. The resistance was calculated from $\Omega = G\,V/I$ where $V$ is the generated voltage, $I$ is the applied current and $G$ is a constant which depends on geometric factors.

For $G$ we have taken a value of 4.24 which corresponds to a sample 20 mm long and 10 mm wide and a spacing of 1 mm for the tips of the probe.[21] The specific resistivity was obtained by multiplying the sheet resistance by the thickness of the layer.

Optical absorption was measured in the wavelength region 400–900 nm using a double beam UV–VIS Lambda 2 Perkin-Elmer spectrometer. The crystallinity of the samples was examined by X-ray diffraction with a Philips PW 1010/1 diffractometer ($\lambda = 1.54$ A) and the surface morphology of the samples was examined by scanning electron microscopy with a JEOL JSM-840A. This device was equipped with a silicon detector for EDX.

## 3 Results and Discussion

### 3.1 Deposition temperature

Fig. 2 shows the variation of thickness as a function of deposition temperature for two different positions in the reactor, with the results in the form of an Arrhenius type plot. The points corresponding to the first substrate nearest to the reactor entrance (designated substrate A), follow a straight line throughout the whole temperature range indicating kinetically controlled growth, whereas the points corresponding to the substrate furthest from the reactor entrance (designated substrate B), show kinetic control at low temperatures (up to 460 °C) with a levelling-off at high temperatures, corresponding to diffusion control. These two different types of behaviour can be understood in terms of the concentration of $SnCl_2$ at the two positions. The filled circles in Fig. 2 will correspond to the position of maximum concentration of reactant, which

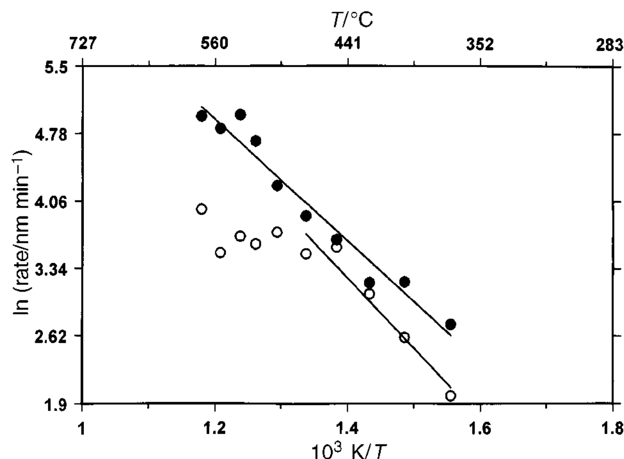


**Fig. 2** Variation of layer thickness as a function of deposition temperature for substrates at 40 cm (●) (substrate A), and at 46 cm (○) (substrate B) from the entrance of the reactor. Deposition time = 20 min.

means a high diffusion flux, allowing kinetic control over the measured temperature range. The open circles in Fig. 2, on the other hand, correspond to a lower concentration of reactant, which means a lower diffusion flux and diffusion control at higher temperatures.

The average value of the activation energy ($E_a$) obtained from the slope in the region with kinetic control for the two lines has a value of 58 kJ mol$^{-1}$. Activation energies have been reported for CVD of $SnO_2$ films for the hydrolysis of tetramethyltin[9] (106.8 kJ mol$^{-1}$) and $SnCl_4$[8] (86.4 kJ mol$^{-1}$). Without a more detailed analysis it is not appropiate to speculate on the mechanistic implications of the lower activation energy for the reaction used here ($SnCl_2 + O_2 \rightarrow SnO_2 + Cl_2$). Previous work[20,22] has reported a mechanism of deposition limited by diffusion for this reaction throughout the temperature range 350–500 °C. This limitation was probably due to the low concentrations of reactant present in the reactor.

Fig. 3 shows the variation of the resistivity of the films on the two substrates A and B as a function of temperature. It can be seen that the specific resistance decreases up to 475–500 °C and then shows a slight increase. The first part of the plot can be explained by the increasing thickness of the layers with deposition temperature. Thicker layers produce an increase in crystallinity of the layers, thus increasing the grain size, decreasing the number of grain boundaries and increasing the conductivity.[23] This could also explain why the filled circles (thicker layers) generally lie below the open circles at each temperature in Fig. 3. The increase at the end of the plot could be explained by a strong decrease in [$Cl^-$], which is introduced by unintentional doping,[23] with increasing substrate temperature. It is also possible, though, that increasing temperature tends to eliminate oxygen vacancies and produce stoichiometric $SnO_2$, thus increasing the resistivity. Studies[24,25] have shown that annealing undoped $SnO_2$ films increases its resistivity by a factor of up to $10^3$ as a result of the elimination of oxygen vacancies. The optimum between the two mechanisms affecting increasing crystallinity and increasing inherent resistivity for our experimental conditions would appear to correspond to a temperature of *ca.* 500 °C. Since this temperature produced the best conducting layers, it was selected for the remainder of the deposition experiments.

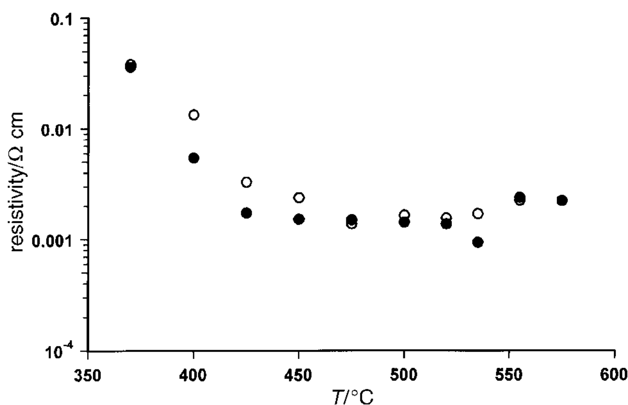


**Fig. 3** Resistivity as a function of deposition temperature for substrates A and B

### 3.2 Deposition rate and electrical properties

Measurement of layer thickness as a function of deposition time for polished silicon substrates at 500 °C showed approximately a linear increase of 83 and 27 nm min$^{-1}$ for substrates A and B, respectively. The sheet resistance decreases with the thickness of the film for a fixed deposition temperature, but with a tendency to a constant value at high thicknesses (Fig. 4). Similar plots[2,4] have been reported previously, but reaching a constant value at lower thicknesses than those found in this work. Grain size has been reported to increase with thickness[4] and this has also been found here (see Section 3.4), but the proportional decrease in the number of grain boundaries compared to the bulk of the material will be much smaller at higher thicknesses. This would explain the tendency of the resistivity to a constant value. The value of $9 \times 10^{-4}$ Ω cm on silicon is a lower figure than those reported[20] for undoped $SnO_2$ films. This indicates adventitious doping of the films by chlorine.

Fig. 5 shows that growth onto Pyrex (squares) compared to those obtained on silicon (circles), gives slightly lower resistivity values. The lowest resistivity measured on Pyrex was $6.4 \times 10^{-4}$ Ω cm compared to $9 \times 10^{-4}$ Ω cm on silicon. This cannot be

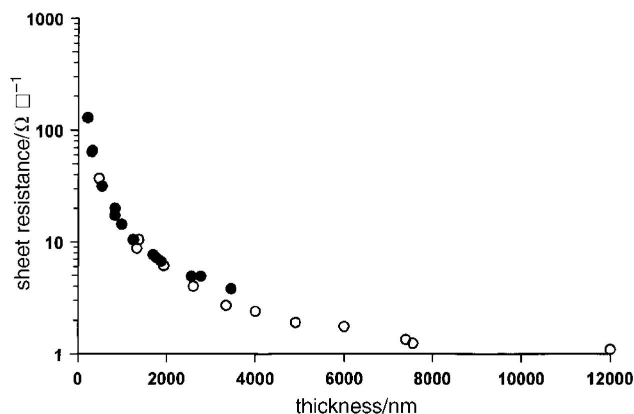


**Fig. 4** Sheet resistance as a function of film thickness for substrates A and B

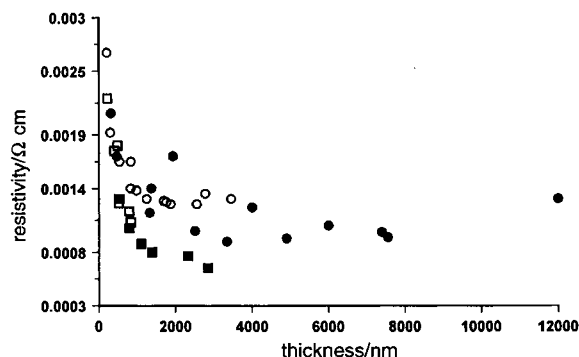


**Fig. 5** Resistivity as a function of film thickness for silicon substrates A and B (●, ○) and for Pyrex glass substrates A and B (■, □)

explained by a low concentration of alkali-metal ions in Pyrex migrating into the $SnO_2$ and acting as a p-dopant because they would in fact neutralise some of the charge carriers.[18] There could, though, be a difference in surface morphology between polished silicon and Pyrex. The Pyrex surface was much more irregular than that of polished silicon and this could allow the growth of bigger grains, producing $SnO_2$ films with lower resistivities.

As mentioned above, the particularly low resistivities for layers both on silicon and Pyrex could be due to the presence of chlorine impurity that could act as a donor. However, EDX analysis carried out on a 12 μm thick sample showed only the presence of Sn. Thus the concentration of any possible impurity must have been lower than the detection limits of EDX which is at the atom% level.

### 3.3 Optical properties

One of the most common applications of $SnO_2$ is as a transparent conductive film in solar cells. So the optical properties of the CVD $SnO_2$ films were assessed. In solar cells both the transmittance and conductivity of the films should be as high as possible. Unfortunately, while increasing thickness means increasing conductivity it also means decreasing transmittance. Therefore the optimum value of these two parameters is established by determining a 'figure of merit'. This was defined for transparent conducting films by Haacke[26] as

$$\Phi_{TC} = Tr^{10}/R_{sh}$$

where

$Tr^{10}$ = transmittance at a particular wavelength to the tenth power and $R_{sh}$ = sheet resistance/Ω □$^{-1}$.

The exponent of 10 is introduced to increase variations in values of *Tr* compared with *R* since *Tr* variations are much smaller than those of *R*. Fig. 6 shows this figure of merit as a function of thickness of the layer for a single wavelength and a wavelength range. The wavelength range represents most of the visible region of the spectrum, but as the maximum of the solar flux is concentrated in the green part of the spectrum[27] at about 600 nm and the spectral response of $SnO_2$/Si cells has also been reported[28] to be a maximum near 600 nm, this wavelength was selected for the studies as well. As can be seen, the figure of merit achieves its maximum for a thickness between 400 and 900 nm, in accord with with previous reports.[4] The maximum values are $9.87 \times 10^{-3}$ □ $\Omega^{-1}$ at 600 nm with a film thickness of 800 nm and $7.1 \times 10^{-3}$ □ $\Omega^{-1}$ for the range 400–800 nm with a film thickness of 525 nm. These figures are higher than those previously reported[29] for $SnO_2$ films with no deliberate doping.

The direct and indirect band gaps of tin oxide can also be determined from transmittance studies. The absorption coefficient ($\alpha$) can be calculated for different wavelengths ($\lambda$) from the transmission spectra using the expression

$$\alpha = (1/t)\ln(1/T)$$

where $T$ = transmittance and $t$ = film thickness.

For direct transmission the absorption coefficient varies as $(h\nu - E_g)^{1/2}$ while for indirect phonon-assisted transitions it varies as $[h\nu - (E'_g - E_{ph})]^2$ where $E_g$ and $E'_g$ are the direct and indirect band gaps, respectively, and $E_{ph}$ is the phonon energy. Fig. 7 shows plots of $\alpha^2$ (top curves) and $\alpha^{1/2}$ (bottom curves) *vs.* photon energy for different films. Extrapolation of both sets of curves in their linear regions to $\alpha = 0$ gives an average value for the direct band gap of $E_g = 4.04$ eV and for the indirect transition energy of $E'_g + E_{ph} = 3.40$ eV. These values were found to be independent of the film thickness and are in agreement with previous values given in the literature.[19]

### 3.4 Crystallinity and surface morphology

X-Ray diffraction analysis of the CVD thin films showed that they were polycrystalline in nature. All the diffraction patterns showed only $SnO_2$ peaks. No SnO phase, as has been reported to occur in $SnO_2$ films,[30] was observed in the films. Orientations found were [110], [101], [200], [211], [220], [002] and [301]. Fig. 8 shows the evolution of the peaks with increasing thickness. In the thin films the [211] orientation is the strongest peak (a) with an increasing intensity of the [200] and [301] peaks as the thickness increases [(b)–(d)]. These two peaks become dominant for thicker films with a tendency for the [200] to predominate (d). This tendency for growth of the [200] orientation for thicker films agrees with previous work.[31,32] A theoretical model[4] has shown that growth along the [200] plane produces films with the lowest resistivity whereas growth along the [110], [211] and [301] orientations produces deep lying trapping centres which decrease the concentration of charge carriers and reduce film conductivity. These trapping centres appear only on the surface of crystallites with [110], [211] and [301] crystallographic orientations, and are associated with a lower oxidation state of Sn. This could also help to explain the high conductivity of the thicker samples grown here.

Fig. 9 shows SEM micrographs which show the evolution of grain size with film thickness increasing from 0.47 to 12 μm [(a)–(h)]. As can be seen the grain size increases monotonically with thickness and grains have a similar shape (*i.e.* preferred orientation) for the crystallites in each picture. This orientation may correspond to the [200] growth seen in the XRDs. This steady growth of grain size with layer thickness has been previously reported,[4] but is in contrast with the more usual behaviour found of grain size saturating at a given thickness.[31,32]

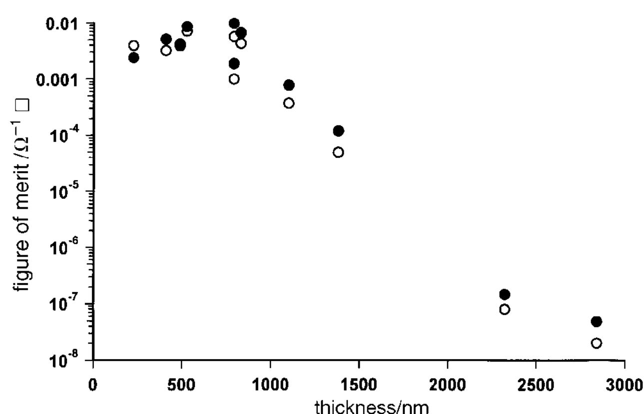


**Fig. 6** Figure of merit as a function of film thickness for 600 nm (●) and 400–800 nm (○)

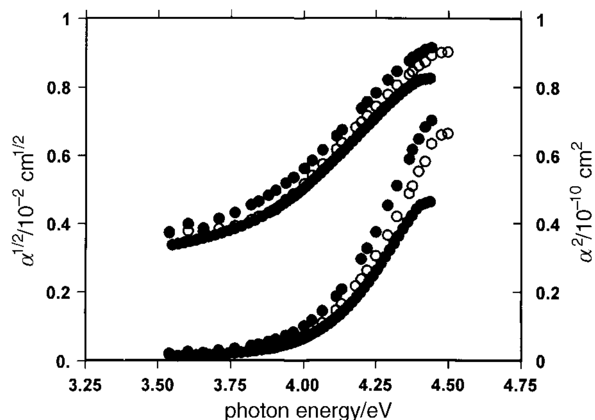


**Fig. 7** Dependence of the square and the square root of the absorption coefficient on photon energy for the different samples

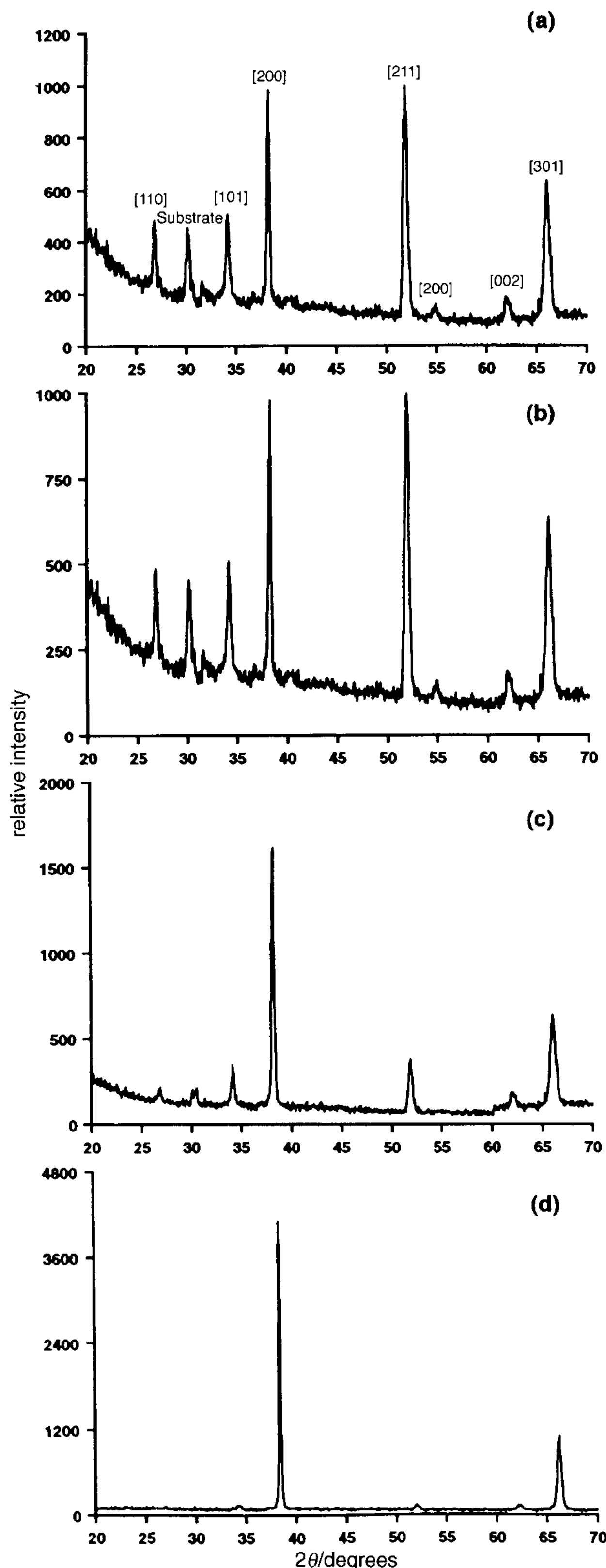

Fig. 8 Evolution of XRD patterns with film thickness

Grain size can be calculated from the XRD patterns using Scherrer's formula[8]

$$D = 0.9\lambda/\beta\cos\theta$$

where $\lambda = 1.54$ Å, $\beta = B - b$, $B$ is the observed width at half of the intensity of the peak at an angle $2\theta$, and $b$ is an instrumental parameter as determined from the broadening of the monocrystal silicon diffraction line. The grain size obtained using this equation was *ca.* 0.4 µm for our thicker films for the [200] orientation. If we compare this value with the size of the crystals seen in the last micrograph in Fig. 9, these appear to be larger than 0.4 µm, but it is difficult to discern exactly the boundary between different monocrystals in the micrographs; it cannot be assumed that each observed structure corresponds to a monocrystal. However, even a grain size of 0.4 µm is larger than any previously reported for both doped and undoped $SnO_2$,[19,22,31,32] which, combined with the preferred growth along the low resistance [200] orientation, could also explain the very low resistivity observed in our samples.

## 4 Doping and electrochemistry

As has been mentioned in the Introduction, $SnO_2$ shows high chemical and electrochemical stability, high electrical conductivity, especially when doped, and a high oxygen evolution overpotential which makes it an interesting alternative electrode to Pt and $PbO_2$ for the oxidation of organic molecules. As already mentioned, Pt electrodes are too expensive for use on an industrial scale and $PbO_2$ is not stable at the low pH generated in an anodic process.[11] Unfortunately, as has been indicated $SnO_2$ has also proved to be unstable and to show disintegration at the high current densities required for industrial applications.[10,11] Similar behaviour has been observed for $SnO_2$ films deposited by spray pyrolysis.[33]

As the resistivity of the undoped $SnO_2$ films was as low as most of the Sb doped $SnO_2$ films which were subsequently produced, initially the stability of the undoped films at a current density of 50 mA cm$^{-2}$ in a 50 g dm$^{-3}$ solution of $Na_2SO_4$ was tested. $SnO_2$ films deposited on heavily doped silicon with a thickness of 4 µm had after 1.5–2 h of electrolysis silicon exposed around the contact area where the $SnO_2$ had totally disintegrated. This appearance was probably due to a non-uniform current distribution in the semiconductor, and to avoid this, 7 µm thick $SnO_2$ films were deposited onto titanium. These films had a 'spotted' surface appearance after 2 h of current flow, with a regular distribution of holes through which oxidised titanium could be seen underneath. To identify possible causes for the breakdown of the $SnO_2$ films a series of experiments were carried out.

Samples left in 9 M HCl for 5 h showed no degradation at all in surface appearance and conductivity, proving their stability at low pH and discounting local high concentrations of $H^+$ at the anode while passing current as the main cause for their disintegration. Samples left in a 2.5 M NaOH solution also showed no change in their properties, proving their stability at high pH.

It has been suggested that $SnO_2$ films are not stable under high current density conditions because ozone is generated and that the films are progressively eroded, probably by the formation of tin(IV) ions;[11] it is interesting to note in this context that $SnO_2$ shows a current efficiency for ozone generation higher than any other common anode material, including $PbO_2$.[10] As $O_3$ is produced on the surface of anodes at high current densities, a current density of 100 mA cm$^{-2}$ was used with two platinum electrodes with the anode placed 0.5 cm underneath the surface of a $SnO_2$ film. Any $O_3$ produced on the platinum anode would have impinged directly on the film. After 3 h with this arrangement the $SnO_2$ film showed no apparent change in its properties, indicating that external erosion or attack by $O_3$ and/or $O_2$, which is produced extensively on the anode, was an unlikely cause for film deterioration.

Reduction of the oxide by diffusion of the hydrogen produced on the platinum counter electrode was unlikely due to the oxidising conditions close to the anode, and also because of the reported[34] strong resistance of $SnO_2$ films against reduction. Nevertheless, to test this possibility, a Nafion membrane was placed in between the electrodes to prevent hydrogen from diffusing onto the anode. The observed degradation of the

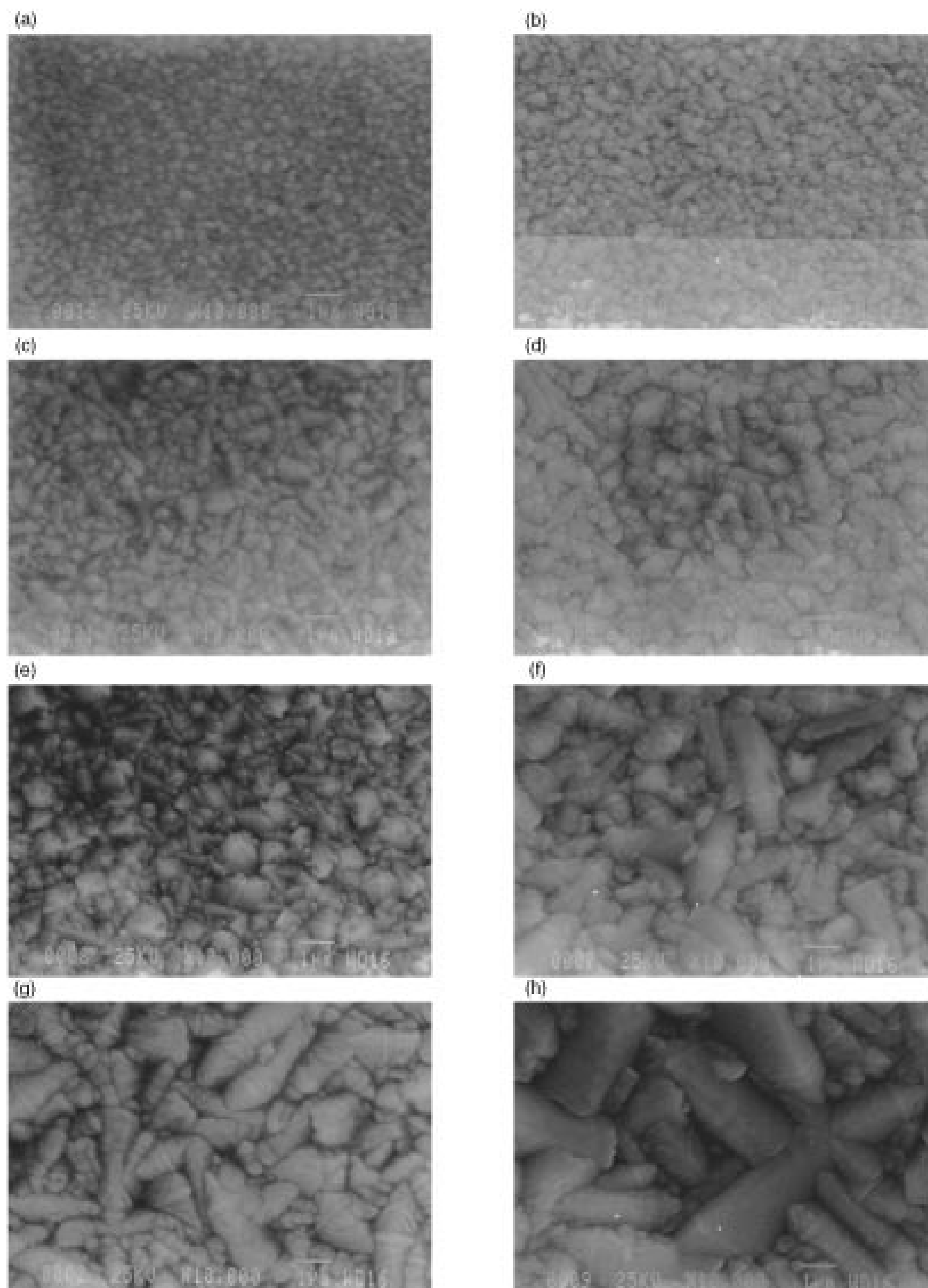

**Fig. 9** SEM pictures showing the evolution of grain size with film thickness

films after 2 h of electrochemical reaction made reduction by $H_2$ as a cause for their degradation unlikely.

Thinner samples were then used as electrodes to check if smaller grain sizes (see Section 3.4 on crystallinity and surface morphology), despite the increasing resistivity, would help improve the performance of the layers. These thinner films disappeared after electrolysis for 30–45 min at 50 mA $cm^{-2}$, thus indicating a relationship between thickness and lifetime of the layers. This is shown more specifically in Fig. 10. These results could suggest a surface process as the reason for the disintegration, since if a process were occurring inside the layer the deterioration would be less dependent on thickness. Surface processes have also been suggested for the observed dissolution of other metal oxides such as $RuO_2$,[35] and $WO_3$[36] in electrochemical applications.

Doping with n-type dopants, such as Sb and F, is known to increase carrier concentration and to improve conductivity by up to three orders of magnitude. Doping has also been reported to improve the lifetime of $SnO_2$ films at high current densities.[10] To test the effect of such a change of the properties on film stability, $SbCl_5$ was introduced into the reaction chamber by passing different flows of $N_2$ (50, 100, 150 and 200 $cm^3$ $min^{-1}$) through a bubbler containing the dopant precursor (see Experimental section). These doped films showed no significant improvement in the resistivity of the samples with a value around $1.1 \times 10^{-3}$ $\Omega$ cm compared to the value of

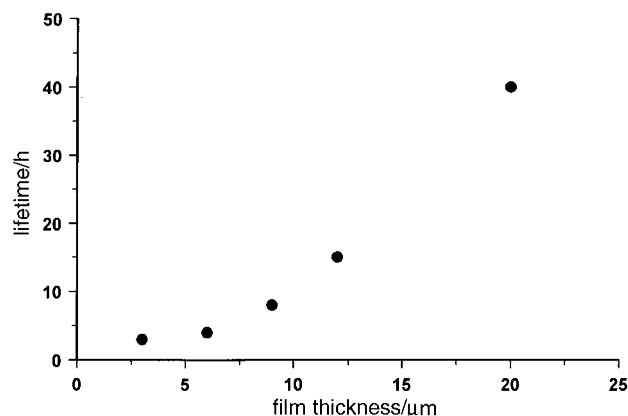


**Fig. 10** Dependence of film lifetime in an electrochemical cell on film thickness

$1.3 \times 10^{-3}$ Ω cm for the undoped ones. Their electrochemical behaviour on passing current was also the same as the undoped ones with similar lifetimes (1–1.5 h) for similar thicknesses (2 µm).

From these experiments it can be concluded that it is unlikely that electrolyte conditions (*e.g.* pH, presence of $O_2$, $O_3$ and $H_2$) on their own are the cause of layer destruction, and although it is still possible that a combination of such factors could contribute to film breakdown this is thought to be unlikely. It is more likely that a process related to the electrochemical oxidation is the main reason for film failure, and this is supported by the fact that the effect is especially noticeable at high current densities. It is interesting to note in this context that when the current was applied the voltage of the cell increased almost immediately up to a value of between 6 and 8 V, depending on the sample, and then remained constant for the rest of the experiment. This observation is in contrast with a reported increase of cell voltage with time,[10] which was explained in terms of migration of $O_2$ through the layer leading to oxidation of the titanium underneath and formation of highly resistive $TiO_2$ with a resulting increase in the potential drop at the electrode. In our case the fact that the resistivity of the electrode did not vary with time would discount $O_2$ diffusion as a possible factor in the break-up of the layers.

The question still remaining is, what is causing the disintegration of the layers? Erosion by $O_2$ and $O_3$ generated at high pressure in small microcrevices could break up the layers even if bubbling of these gases over a layer has no effect. Alternatively, generation of reaction intermediates able to combine with the oxide could dissolve the films, probably in the form of tin(IV) ions as a result of the oxidising conditions.[10,11] Instability of the layer could also arise with high current densities as a result of localised heating and strains produced at grain boundaries. These boundaries are high-energy areas because of the multidirectional growth of the crystals and the presence of impurities which tend to migrate there. High current densities can destabilise the boundaries and break up the layers. The overall degradation of the films could be the result of any one of these factors or a combination of them.

## 5 Conclusions

$SnO_2$ films have been successfully prepared by CVD by reaction of $SnCl_2$ with $O_2$, using an evaporator inside the reactor as the precursor source. A value for the activation energy, $E_a$, of 58 kJ mol$^{-1}$ has been determined for the reaction. A temperature range of 450–500 °C has been found to be optimum for the deposition of the layers. Resistivities of the films of $9 \times 10^{-4}$ Ω cm on silicon and $6 \times 10^{-4}$ Ω cm on Pyrex are the lowest reported so far for deliberately undoped $SnO_2$ films. A figure of merit of $9.87 \times 10^{-3}$□ $\Omega^{-1}$ for a 0.8 µm thick film is also the highest reported so far. Characterisation of the films by XRD showed a preferred [211] orientation and the grain size obtained from the XRD and also from SEM micrographs was larger than 0.4 µm. However, the $SnO_2$ films, as also reported by others, were unstable in a electrochemical cell. It has been suggested that an electrochemical process is the main cause for the disintegration. A more detailed electrochemical investigation is now underway.

The work in this paper was carried out with the support of EA Technology Ltd funded through the Core Research Programme and partially by the Basque Government *via* a scholarship of the Research Training Programme of the Department of Education, Universities and Research.

### References

1 H. De Waal and F. Simonis, *Thin Solid Films*, 1981, **77**, 253.
2 H. Haneko and K. Miyake, *J. Appl. Phys.*, 1992, **53**, 3629.
3 P. S. Reddy, S. Uthanna and P. J. Reddy, *J. Vac. Sci. Technol. A*, 1987, **5**, 1688.
4 D. Belanger, J. D. Dodelet, B. A. Lombos and J. I. Dickson, *J. Electrochem. Soc.*, 1985, **132**, 1398.
5 A. Rohatgy, T. R. Viverito and L. H. Slack, *J. Am. Ceram. Soc.*, 1974, **57**, 6.
6 B. J. Baliga and S. K. Ghandi, *J. Electrochem. Soc.*, 1976, **123**, 941.
7 C. G. Granquist, *Appl. Phys. A*, 1993, **57**, 19.
8 G. Sanon, R. Rup and A. Monsingh, *Thin Solid Films*, 1990, **190**, 287.
9 T. P. Chow, M. Ghezzo and B. J. Baliga, *J. Electrochem. Soc.*, 1982, **129**, 1041.
10 R. Kotz, S. Stucki and B. Carcer, *J. Appl. Electrochem.*, 1991, **21**, 14.
11 P. C. Foller and C. W. Tobias, *J. Electrochem. Soc.*, 1982, **129**, 506.
12 J. P. Marton and D. A. Lepic, *J. Electrochem. Soc.*, 1976, **123**, 234.
13 N. Miyata and H. Kitahata, *Thin Solid Films*, 1985, **125**, 33.
14 T. Feng, A. K. Ghosh and C. Fishman, *J. Appl. Phys.*, 1979, **50**, 8070.
15 T. M. Uen, K. F. Huang, M. S. Chen and Y. S. Gow, *Thin Solid Films*, 1988, **158**, 69.
16 D. E. Carlson, *J. Electrochem. Soc.*, 1975, **122**, 1334.
17 Y. S. He, J. C. Campbell, R. C. Murphy, M. F. Arendt and J. S. Swinnea, *J. Mater. Res.*, 1993, **8**, 3131.
18 J. Kane, H. P. Schweizer and W. Kern, *J. Electrochem. Soc.*, 1975, **122**, 1144.
19 R. D. Torey and T. A. Raju, *Thin Solid Films*, 1985, **128**, 181.
20 N. S. Murty, G. K. Bhogavat and S. R. Jawalear, *Thin Solid Films*, 1982, **92**, 347.
21 F. M. Smits, *Bell Systems Tech. J.*, 1958, **37**, 711.
22 N. S. Murty and S. R. Jawalear, *Thin Solid Films*, 1983, **102**, 283.
23 J. Bruneaux, H. Cachet, M. Froment and A. Messad, *Electrochim. Acta*, 1994, **39**, 1251.
24 J. Kane, H. P. Schweizer and W. Kern, *J. Electrochem. Soc.*, 1976, **123**, 270.
25 A. F. Caroll and L. H. Slack, *J. Electrochem. Soc.*, 1976, **123**, 1889.
26 G. Haacke, *J. Appl. Phys.*, 1976, **47**, 4086.
27 H. J. Hovel, R. K. Willardson and A. C. Beer, *Semicond. Semimet.*, 1975, **11**, 86.
28 T. Nagatome, M. Endo and O. Omote, *Jpn. J. Appl. Phys.*, 1979, **18**, 103.
29 C. J. Giunta, D. A. Strickler and R. G. Gordon, *J. Phys. Chem.*, 1993, **97**, 2275.
30 M. Hecq, A. Dubois and J. Van Cakenberghe, *Thin Solid Films*, 1963, **18**, 117.
31 G. Sanon, R. Rup and A. Monsingh, *Phys. Status Solidi*, 1991, **128**, 109.
32 D. J. Goyal, C. Agashe, B.R. Morathe, M. G. Takwale and V. G. Bhide, *J. Appl. Phys.*, 1993, **73**, 7520.
33 D. Gilroy, personal communication.
34 G. B Hoflund, *Chem. Mater.*, 1994, **6**, 562.
35 G. Barral, J. Guitton, C. Montella and F. Vergara, *Surf. Technol.*, 1979, **8**, 113.
36 M. S. El-Basiouny, S. A. Hassan and M. M. Hefny, *Corrosion Sci.*, 1980, **20**, 909.

*Paper* 6/08525C; *Received* 23rd *December*, 1996